(Received 31 October 2025, Accepted 24 November 2025, Scheduled 20 December 2025)

Miniaturized Wideband Filtering Antenna without Additional Filtering Structures

Li Wang[1], Han Lin[1,*], and Chenlu Li[2]

[1] School of Electrical and Information Engineering, Anhui University of Science and Technology, Huainan 232001, China
[2] School of Electrical and Information Engineering, Hefei Normal University, Hefei 230061, China

ABSTRACT: This paper proposes a single-layer, low-profile, and compact filtering patch antenna. The antenna requires no additional filtering structures and consists only of a dielectric substrate, a radiating patch etched with both star-shaped slots and L-shaped slots, a feeder line integrated with a quarter-wavelength matching stripline, and a partial ground plane connected to inverted-π branches. Among these components, the radiating patch, feeder line, and inverted-π branches work synergistically to form two radiation nulls on either side of the passband. This not only enhances the frequency selectivity at the band edges but also optimizes the antenna's radiation performance and filtering performance simultaneously. Finally, to verify the validity of the design, a prototype of the antenna is designed, fabricated, and tested, and the measured results are in good agreement with the simulated results. The design achieves a wide impedance bandwidth of 66.5% (2.33–4.65 GHz), a peak realized gain of 4.25 dBi, and an average efficiency of up to 92%. With a size of 35 mm $\times$ 29 mm $\times$ 0.8 mm, the antenna satisfies the miniaturization requirement and can be applied to various scenarios, including short-range wireless communication and 5G communication.

1. INTRODUCTION

With the development of modern wireless communication systems toward high integration, the demand for high integration and miniaturization of radio frequency (RF) front-end components has become increasingly urgent. As key front-end components, filters and antennas directly determine the system's signal transmission quality and space utilization efficiency. Furthermore, the evolution of wireless communication technology requires achieving high-quality communication in small spaces, which makes bandwidth a core consideration in antenna design. In traditional designs, filters and antennas are usually connected as independent components via matching networks. This design inevitably introduces high insertion loss, structural redundancy, and electromagnetic compatibility (EMC) issues, making it difficult to meet the requirements of modern communication devices for compact structures and high performance. In recent years, filtering antennas, a new type of RF device that deeply integrates radiation and filtering functions, have emerged. Currently, various types of filtering antennas have been proposed, including filtering slot antennas, filtering patch antennas, filtering dipole antennas, and filtering dielectric resonator antennas (DRAs). Such antennas can simultaneously realize signal transmission and reception in a single radiating unit, and possess out-of-band interference suppression capability. They effectively reduce the number of cascaded modules, significantly improve system integration and overall efficiency, thus emerging as one of the key solutions to address the aforementioned technical challenges.

There are two main design methods for filtering antennas. One involves cascading the filter and the antenna via transmission lines following their separate design [1–3], and the other entails the co-design of the filter and the antenna, in which the last-stage resonator of the filter is substituted with the radiating patch of the antenna [4–8]. With respect to the first design method, Reference [1] presents a filtering antenna, achieved by directly connecting the patch to the output port of a hairpin filter via through-holes. The patch and the filter share a common ground, a feature that enhances the compactness of the entire device. However, this method requires the separate design of the antenna and the filter, various resonators and filters are typically employed to feed the patch antenna, thereby enabling both radiation and filtering functionalities. In addition, such designs generally exhibit narrow bandwidth and inevitably incur insertion loss, which in turn leads to a decrease in antenna gain. Regarding the second method, Ref. [4] presents a filtering slot antenna. By loading a multi-mode resonator to excite the slot antenna, the device achieves both wideband operation and high selectivity simultaneously. Ref. [7] develops a filtering patch antenna by etching straight slots of varying lengths into the patch and introducing two near-band radiation nulls. In [8], an inverted L-shaped antenna serves as both the radiator of a parallel coupled-line filter and the final resonator, thus realizing a third-order Chebyshev bandpass filtering response. While this method can achieve excellent filtering performance, the insertion loss associated with complex filtering circuits may cause reductions in both antenna gain and efficiency — an outcome that hinders device miniaturization. Therefore, filtering antennas that integrate antenna-filter functionalities have emerged as mainstream research direction.

This integrated design can be realized via various technical approaches, such as adopting metasurface designs [9, 10], stacked patch designs [11, 12], loading parasitic

* Corresponding author: Han Lin (hanlin@aust.edu.cn).

patches [13, 14], loading shorting probes [15–17], utilizing slotted patches [18, 19], and employing defected ground structures (DGS) [20, 21]. These methods generate radiation nulls on both sides of the antenna's operating frequency band, thus endowing the antenna with filtering capability. Ref. [10] proposes two novel types of dual-polarized filtering metasurface antennas. Their design employs uniformly arranged square metasurface structures combined with polarization cross-slots, and incorporates short truncated lines and etched slots into the metasurface structures to create radiation nulls on both sides of the passband. Ultimately, the out-of-band rejection ratio exceeds 30 dB. Ref. [12] designs a compact, low-profile linearly and circularly polarized filtering stacked patch antenna operating in the 2.0 GHz frequency band. It employs customized inverted Y-shaped coupling probes to achieve filtering functionality. Nevertheless, this stacked patch antenna features a complex design and a narrow impedance bandwidth, and leads to increased manufacturing costs and complexity. Ref. [14] presents a compact wideband filtering antenna with high selectivity. This antenna achieves a 21.5% impedance bandwidth and generates three radiation nulls through loading parasitic patches and etching coupling slots on the ground plane for feeding purposes. However, this antenna imposes high requirements on manufacturing precision and presents significant difficulty in optimization. In [17], the antenna is fed via an F-shaped probe, and cross-coupling is introduced within the antenna, thereby generating two symmetric radiation nulls on both sides of the passband and thus developing a filtering patch antenna. However, this antenna has a narrow usable bandwidth, a complex design, and cannot meet the miniaturization requirements. Therefore, for filtering antennas with an integrated design, achieving an optimal balance between a simple and compact structure, wideband characteristics, and excellent radiation performance remains an important challenge to be addressed at present.

Compared with traditional design methods, the integrated design approach eliminates the need for a separate filtering structure [22, 23, 25]. For instance, the design in reference [23] can achieve superior filtering performance while maintaining antenna gain by fine-tuning specific parameters to adjust the bandwidth and control the radiation null location. Based on this integrated design paradigm, this paper proposes a miniaturized wideband filtering antenna without the need for an additional filtering structure. The antenna employs a single-layer design, characterized by a compact profile, a wide usable bandwidth, and a flat gain response within the passband, besides, this antenna exhibits good out-of-band rejection and outstanding filtering performance. Finally, to further investigate and validate the radiation and filtering performance of the antenna in detail, a physical prototype of the proposed antenna was fabricated and tested. Special emphasis was placed on analyzing the generation mechanism of the radiation nulls and the impact of the specially designed parameters. Experimental results indicate that the measured results are basically consistent with the simulated results. Furthermore, this antenna can effectively cover a range of key frequency bands, including unlicensed industrial, scientific, and medical (ISM) bands, primary 5G New Radio (NR) bands, and short-range communication bands. It holds broad application potential in domains including healthcare (leveraging ISM bands), radar and remote sensing, the Internet of Things (IoT), short-range communications, aerospace, and the low-altitude economy, as well as industrial control.

2. ANTENNA DESIGN

2.1. Antenna Configuration

The overall structure and detailed dimensions of the proposed filtering antenna are illustrated in Figure 1. This antenna is printed on a single-layer dielectric substrate, comprising a top layer and a bottom layer. This design employs an FR4 substrate with a relative permittivity of 4.4 and a loss tangent of 0.02, and the antenna exhibits an overall dimension of 35 mm × 29 mm × 0.8 mm.

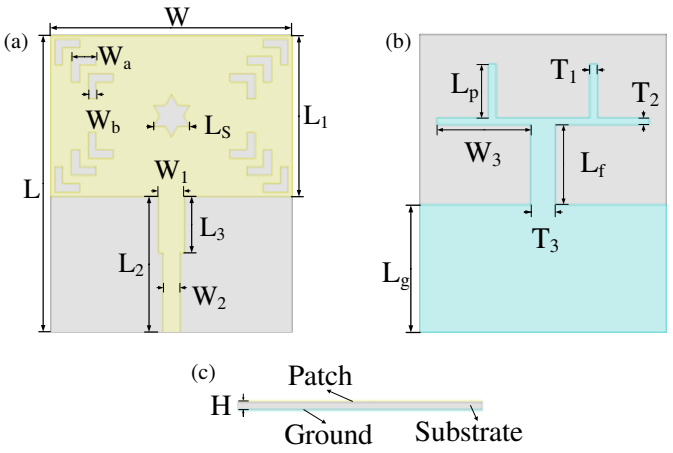

FIGURE 1. Configuration of the proposed filtering antenna. (a) Top view. (b) Bottom view. (c) Side view.

As illustrated in Figure 1(a), the top layer consists of two parts. The upper part is the main radiating patch, which features a hexagram-shaped slot at its center and three sets of L-shaped slots distributed at the four corners of the rectangular patch; the lower part is connected to a microstrip feed line integrated with a quarter-wavelength impedance-matching line, employs a 50 Ω microstrip line for feeding, and its primary function is to enhance the antenna's impedance matching performance. As illustrated in Figure 1(b), the bottom layer employs a branched configuration: the lower part functions as the main grounding segment of the antenna, while the upper part is connected to an inverted π-shaped branch. This branched structure is utilized to enhance impedance matching, regulate current distribution, and thus optimize the antenna's overall performance. In addition, the slots and feed line on the antenna's front side work synergistically with the inverted π-shaped branch and defected ground plane (DGP) on its back side. This synergy enables the precise localization of two radiation nulls at the upper and lower edges of the passband gain response, thereby enhancing the out-of-band signal rejection capability. Finally, the proposed filtering patch antenna exhibits a compact structure and realizes a filtering response without the need for additional filtering components. The final optimized dimensional parameters of the antenna are summarized in Table 1.

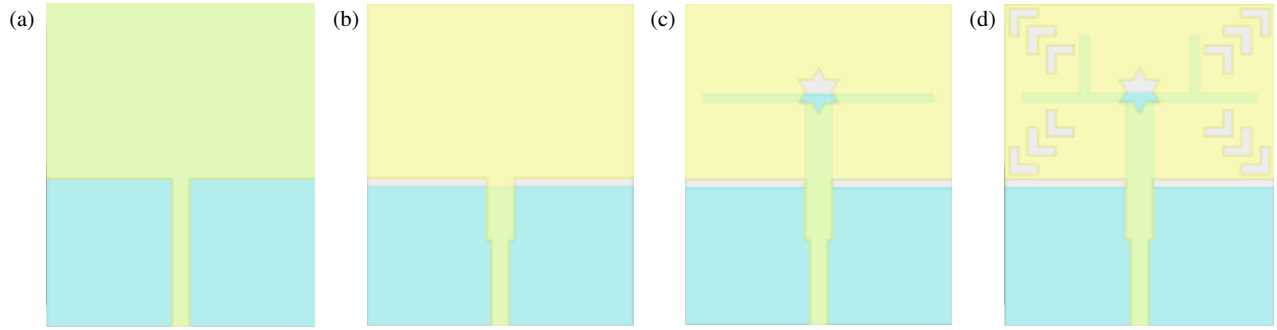

FIGURE 2. Evolution of the proposed filtering antenna. (a) Reference Antenna I. (b) Reference Antenna II. (c) Reference Antenna III. (d) Proposed Antenna IV.

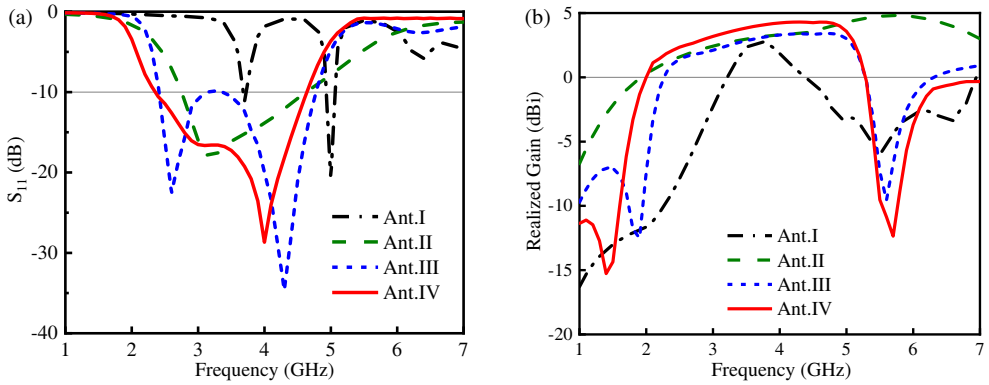

FIGURE 3. Simulated results of four antennas. (a) S_{11}. (b) Peak realized gain.

TABLE 1. Dimensions of filtering antenna.

Parameter	W	W_a	W_b	W_1	W_2	W_3	L	L_s	L_1
Value (mm)	29	3	1	3	2	11.1	35	4.33	19
Parameter	L_2	L_3	L_g	L_f	L_p	T_1	T_2	T_3	H
Value (mm)	16	6.7	15	9.4	6.3	0.9	0.8	2.8	0.8

2.2. Antenna Design Process

To further illustrate the design process and operating principle of the proposed antenna, Figure 2 illustrates the evolution process of the proposed filtering patch antenna. Reference Antenna I serves as the initial structure, which is a basic rectangular microstrip patch antenna consisting solely of a rectangular radiating patch and a bottom layer. Reference Antenna II is improved based on Antenna I, with the specific modification of adding a quarter-wavelength impedance-matching line to the front end of the microstrip feed line and optimizing the length of the bottom layer. Reference Antenna III is a further modification based on Antenna II, with two key adjustments: first, a hexagram-shaped slot is etched at the center of the rectangular radiating patch; second, a "T"-shaped branch is added above the bottom layer. The proposed Antenna IV is a further optimization based on the third reference antennas, with two optimizations: first, three sets of "L"-shaped slots are etched at the four corners of the rectangular radiating patch; second, the branch on the bottom layer is modified from the original "T"-shape to the final inverted π-shape.

Figure 3 illustrates the simulated curves of S-parameters and realized gain for the three reference antennas and the proposed filtering antenna. As shown in Figure 3(a), Reference Antenna I exhibits three resonant frequencies at 3.7 GHz, 5.0 GHz, and 6.3 GHz, but its impedance bandwidth with a return loss below -10 dB is relatively narrow. Furthermore, as observed in Figure 3(b), the maximum peak gain of Reference Antenna I is only 2.7 dBi; thus, Reference Antenna I lacks a filtering effect.

For Reference Antenna II, a quarter-wavelength impedance matching line is added to the microstrip feed line, and the dimensions of the ground plane are optimized. This antenna only excites one resonant frequency at 3.2 GHz, with its operating bandwidth expanded to 48.5% (2.78–4.56 GHz). Upon observation of Figure 3(b), the gain of Reference Antenna II increases gradually within the target frequency band and only exhibits a downward trend after 5.7 GHz. Compared with Reference Antenna I, Reference Antenna II exhibits a degree of filtering functionality, but it fails to achieve satisfactory out-of-band suppression performance. Therefore, further optimization is required to enhance the antenna's out-of-band suppression performance.

To enhance the filtering response characteristics of the antenna and improve out-of-band suppression performance, a star-shaped slot is etched on the rectangular radiating patch of Reference Antenna II, and a "T"-shaped branch is added to the bottom layer, resulting in the development of Reference Antenna III. As shown in Figure 3(a), after these modifications, the operating bandwidth of the antenna is slightly wider than that

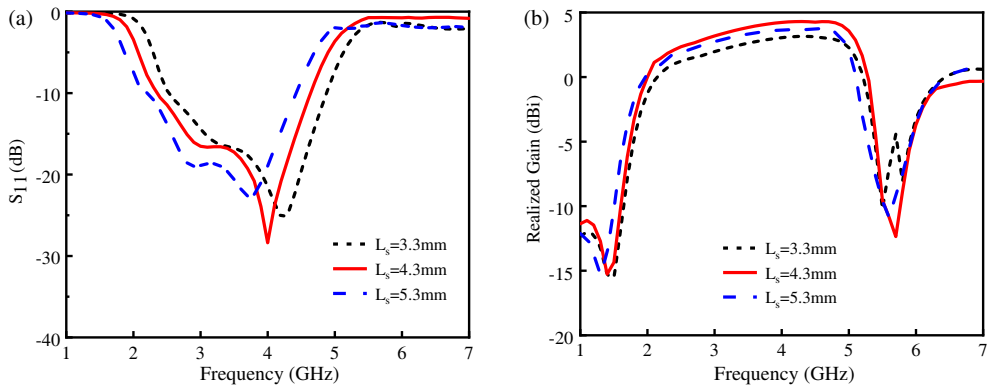

FIGURE 4. Simulated (a) S_{11} and (b) peak realized gain of the filtering antenna for different lengths of L_s.

of the original (Reference Antenna II), and two resonant frequencies are observed at 2.6 GHz and 4.3 GHz. On both sides of the low-frequency and high-frequency resonant frequencies, the S_{11} curve exhibits a steep downward trend and a steep upward trend, respectively. However, the S_{11} value increases to -9.82 dB at 3.2 GHz, indicating suboptimal impedance matching performance. When combined with the results in Figure 3(b), the gain of Reference Antenna III is stable within the operating frequency band. Compared with Reference Antenna II, its high-frequency out-of-band suppression level is significantly improved, and a more pronounced filtering effect is generally achieved. Nevertheless, the impedance matching performance in certain aspects still requires enhancement.

Finally, three sets of "L"-shaped slots are etched at each of the four corners of the main radiating patch of Reference Antenna III, and targeted adjustments are subsequently performed on the bottom layer structure of the aforementioned antenna to develop the proposed Antenna IV. This improvement enables the proposed antenna to operate at two adjacent resonant frequencies (3.0 GHz and 4.0 GHz), exhibiting corresponding return losses of -16.5 dB and -28.2 dB, respectively. Based on the -10 dB return loss criterion, the proposed Antenna IV exhibits an impedance bandwidth of approximately 65.7% (2.35–4.65 GHz). As shown in Figure 3(b), the gain of the proposed antenna increases gently within the passband, with a maximum gain of 4.27 dBi. At the lower and upper radiation nulls (located around 1.4 GHz and 5.7 GHz, respectively), the antenna exhibits notable out-of-band suppression performance, and the proposed Antenna IV generally exhibits excellent filtering performance.

2.3. Parametric Study

To further understand the operating mechanism of the proposed filtering antenna, this study analyzes selected parameters. It was observed that the filtering performance of the proposed antenna is significantly affected by the side length L_s of the star-shaped slot and the vertical length L_f of the rectangular strip below the π-shaped stub. Thus, this section presents a detailed analysis of parameters L_s and L_f. Figures 4 and 5 respectively show the simulated curves of S_{11} and peak gain corresponding to different values of L_s and L_f.

As shown in Figure 4(a), as L_s increases from 3.3 mm to 4.3 mm, a new resonance frequency appears at the low frequency (3 GHz). As L_s increases from 4.3 mm to 5.3 mm, the S_{11} value at the low-frequency resonance frequency decreases from -16.3 dB to -19.5 dB. Additionally, as L_s increases from 3.3 mm to 5.3 mm, the center frequency shifts downward from 4.2 GHz to 3.7 GHz. This indicates that L_s primarily influences the amplitude of the low-frequency resonance frequency. From Figure 4(b), it can be observed that as L_s increases from 3.3 mm to 5.3 mm, the antenna's peak gain exhibits a trend of first increasing and subsequently decreasing; however, the low- and high-frequency radiation nulls remain largely unchanged. This confirms that L_s also affects the antenna's gain.

As shown in Figure 5(a), as L_f increases from 8.4 mm to 10.4 mm, the antenna's overall operating frequency shifts toward the lower frequency range. Meanwhile, Figure 5(b) shows that as L_f increases from 8.4 mm to 9.4 mm, the low-frequency radiation null also shifts toward lower frequencies; however, further increases in L_f result in negligible changes to the low-frequency radiation null. Similarly, increasing L_f causes the antenna's high-frequency radiation null to shift toward lower frequencies. Thus, L_f primarily affects the antenna's operating frequency range and the positions of the high-frequency radiation nulls.

2.4. Working Principle

To further clarify the working principle of the proposed filtering antenna, this section presents a detailed analysis of the generation mechanism of the radiation nulls at the lower and upper edges of the passband. Figure 6 shows the vector current distribution of the proposed filtering antenna, providing a reference for understanding the formation mechanism of the two radiation nulls (at 1.4 GHz and 5.7 GHz). From Figure 6(a), it is evident that at 1.4 GHz, surface current is primarily concentrated near the rectangular strip connecting the feed point to the star-shaped slot, while the surface current in other regions is weak; meanwhile, surface current on the antenna ground plane is also primarily concentrated in this region and exhibits an opposite direction. This precise mechanism leads to the mutual cancellation of magnetic fields within a certain space, thereby forming a radiation null in the low-frequency band.

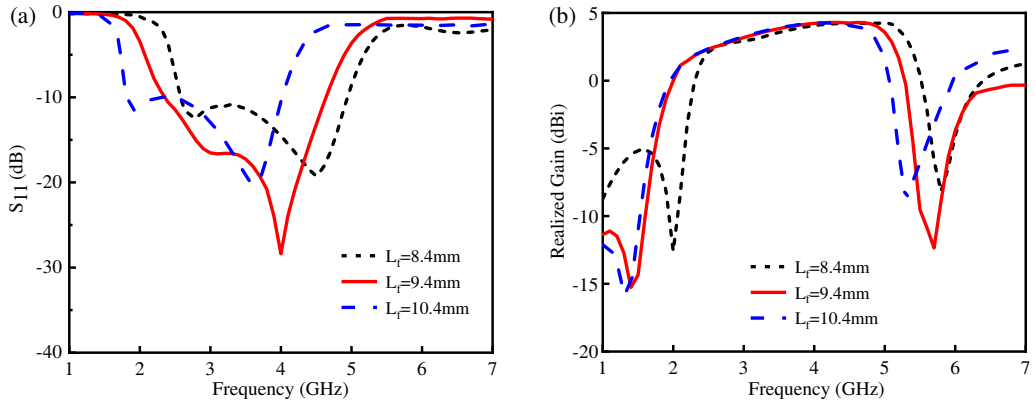

FIGURE 5. Simulated (a) S_{11} and (b) peak realized gain of the filtering antenna for different lengths of L_f.

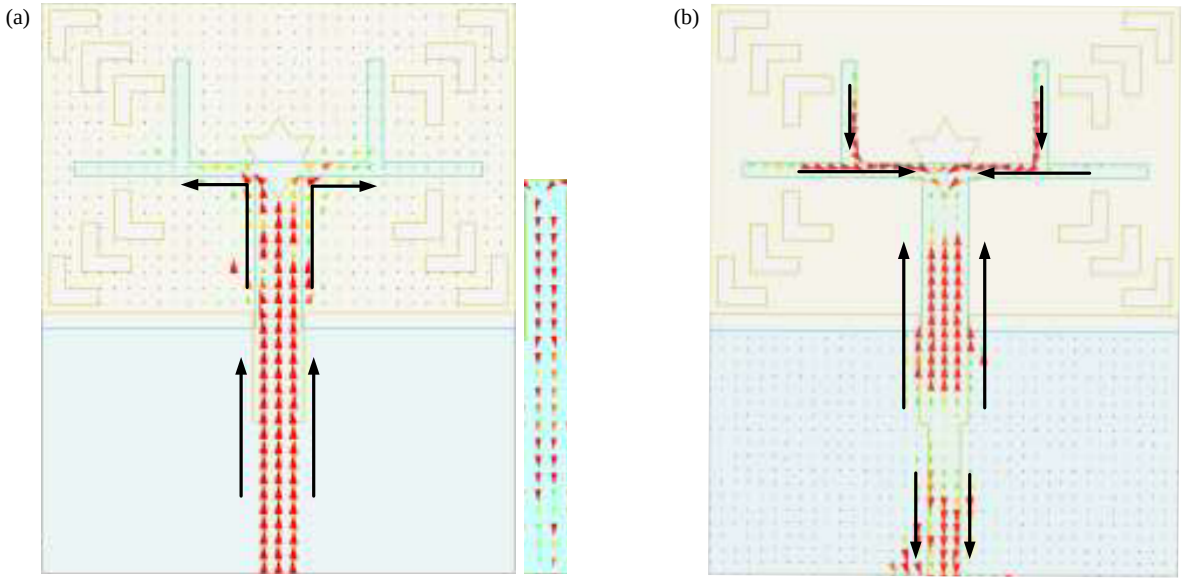

FIGURE 6. Simulated vector current distributions at (a) 1.4 GHz and (b) 5.7 GHz.

Figure 6(b) shows that when the antenna operates at the upper stopband radiation null frequency (5.7 GHz), the currents on the two vertical branches of the inverted π-shaped stub flow downward, converge with the current on the horizontal branch of the stub, and then flow toward the midpoint of the stub. Meanwhile, upward-directed currents are distributed on the lower rectangular strip; these three current components converge below the center of the inverted π-shaped stub and undergo mutual cancellation. These observations indicate that the high-frequency radiation null is attributed to the synergistic effect of reverse currents on the symmetric vertical branches and reverse currents between the stub and the lower rectangular strip.

Figure 7 depicts the equivalent circuit model of the proposed filtering antenna, where Circuit 1 consists of the bottom-side inverted π-shaped branch. Serving as the core of the entire circuit, this component determines the antenna's operating frequency band and suppresses out-of-band interference signals. Circuit 2 comprises the top-side radiating patch and feedline, which serves to convert the filtered signals into electromagnetic waves for transmission and ensure reliable impedance match-

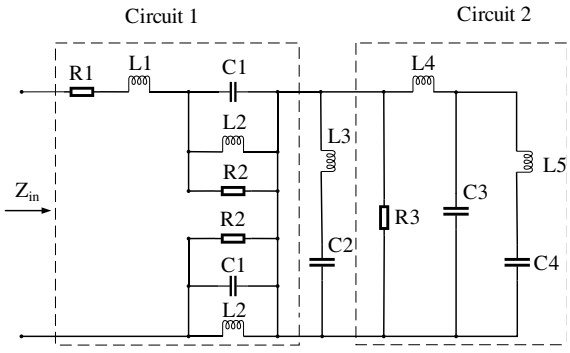

FIGURE 7. Equivalent circuit of the proposed filtering antenna.

ing between the antenna and the filtering structure. Within the circuit, L_1 and C_1 exhibit series resonance, which couples to L_2 to generate the first low-frequency resonant frequency; C_2 and L_3 exhibit series resonance to produce a second resonant frequency, with subsequent coupling to Circuit 1 forming a wider passband. R_3 represents the intrinsic resistance of the radiat-

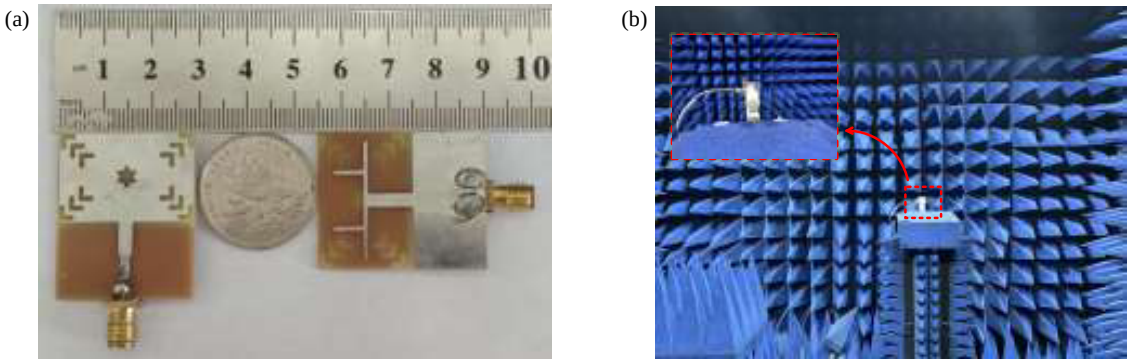

FIGURE 8. Photographs of (a) the fabricated antenna and (b) the measurement environment.

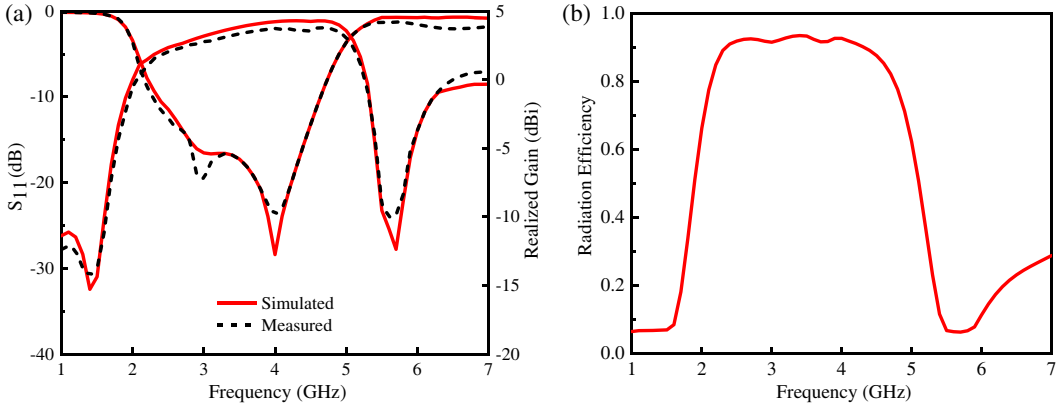

FIGURE 9. Simulated and measured S_{11}, realized gains, and radiation efficiency of the filtering antenna. (a) S_{11} and realized gains (b) Radiation efficiency.

ing patch itself, while L_4 is configured to compensate for the capacitive input impedance of the antenna, rendering it purely resistive across the operating frequency band, thereby enabling maximum power transfer. C_3 corresponds to the star-shaped slot at the center of the patch, and C_4 together with L_5 form a series resonance that represents four sets of L-shaped slots. By tuning the parameters of C_3, C_4, and L_5, the antenna's impedance matching can be optimized to achieve enhanced filtering performance.

3. SIMULATED AND MEASURED RESULTS

The proposed filtering antenna was fabricated and tested. During the design process, High Frequency Structure Simulator (HFSS), a specialized electromagnetic simulation tool, was employed to conduct simulation and optimization. Figure 8(a) presents the physical prototype of the fabricated miniaturized wideband filtering antenna. The antenna is fed via an SMA coaxial connector at the end of the side-fed microstrip line, featuring a compact structure. Additionally, it adopts a symmetric multi-slot layout, endowing it with an aesthetic and novel configuration. The reflection coefficient and far-field radiation characteristics of the antenna were tested using an AV3629D vector network analyzer and an microwave radio darkroom, the testing setup is presented in Figure 8(b).

Figure 9(a) depicts the simulated and measured return loss (S_{11}) and realized gain of the proposed filtering antenna, while Figure 9(b) presents the antenna's radiation efficiency. As shown in Figure 9(a), the simulated and measured impedance bandwidths, defined by a return loss (S_{11}) below -10 dB are 65.7% (2.35–4.65 GHz) and 66.5% (2.33–4.65 GHz), respectively. Moreover, two resonant frequencies of the antenna are more distinctly observed in the measured results. Within the passband, the antenna's gain curve exhibits a steady upward trend; the simulated and measured peak gains are 4.27 dBi and 4.25 dBi, respectively. Two radiation nulls are observed on both sides of the passband, resulting in a steep frequency roll-off. In addition, the frequency ranges where $S_{11} < -10$ dB and gain > 0 dB are consistent between the simulated and measured curves, confirming the proposed antenna's excellent filtering performance. Meanwhile, Figure 9(b) shows that the simulated radiation efficiency of the antenna is approximately 90% within the passband. This efficiency curve exhibits a trend similar to that of the gain curve (with both rising and falling characteristics) and also features two nulls, indicating the antenna possesses high efficiency and excellent selectivity. Overall, the simulated and measured results are in good agreement. Minor discrepancies are primarily attributed to fabrication tolerances and testing environmental conditions.

The normalized realized gain patterns of the proposed miniaturized wideband filtering antenna were measured in the XOZ

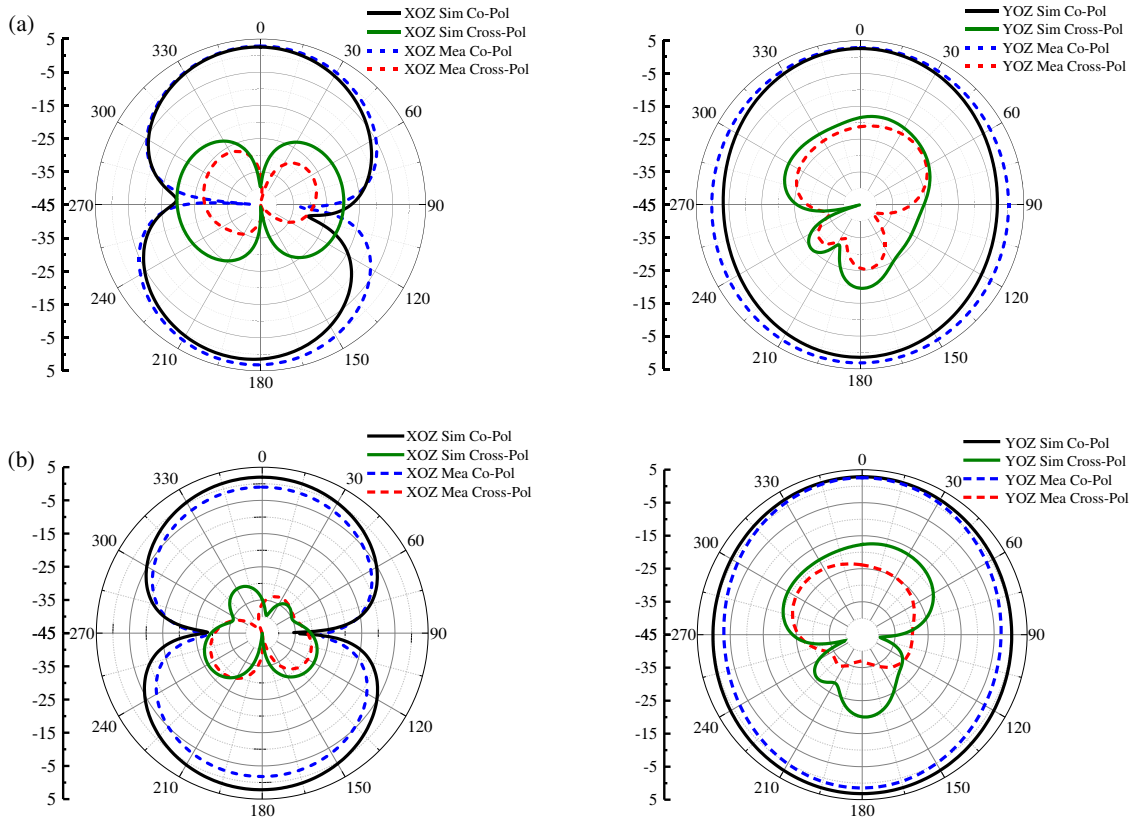

FIGURE 10. Simulated and measured radiation patterns of the filtering antenna in both XOZ and YOZ planes at different frequencies. (a) 3 GHz. (b) 4 GHz.

TABLE 2. Comparison with other reported filtering antennas.

Ref.	Size (mm^2) & (λ_0^2)	Operating Frequency (GHz)	BW (%)	Gain (dBi)	Radiation efficiency (%)
[7]	42×43 (0.51×0.53)	2.63–4.59	54.3	6.44	88.9
[12]	68×68 (0.21×0.19)	1.92–2.05	6.5	5.8	NG
[14]	25×25 (0.41×0.41)	4.53–5.55	21.5	4.8	93
[22]	100×100 (1.23×1.23)	3.15–4.25	29.7	9.5	NG
[23]	35×29 (0.65×0.54)	4.67–6.53	33.2	4.92	NG
[24]	30.9×30.9 (0.49×0.49)	4.08–5.41	28	4.9	93
[25]	44×44 (0.52×0.52)	3.49–4.37	22.4	2.7	NG
[26]	66.5×50 (0.63×0.74)	2.71–2.97	9.2	5.75	NG
Proposed	35×29 (0.41×0.34)	2.33–4.65	66.5	4.25	92

and YOZ planes at two resonant frequencies (3 GHz and 4 GHz) in an microwave radio darkroom. The measurement results are shown in Figure 10, and the figures indicate that the measured and simulated radiation patterns are in good agreement. At 3 GHz and 4 GHz, the radiation patterns in the XOZ plane both exhibit a typical figure-eight pattern, while those in the YOZ plane all exhibit a circular or near-circular pattern. This confirms that the antenna exhibits uniform radiation characteristics in the YOZ plane. Furthermore, at the two resonant frequencies, the simulated and measured co-polarization and cross-polarization in the XOZ and YOZ planes remain well maintained.

4. PERFORMANCE COMPARISON

To highlight the advantages of the proposed filtering patch antenna, Table 2 provides a performance comparison between the proposed antenna and other filtering antennas reported in recent

literature. As indicated by the data in Table 2, the antenna proposed in this study features a simple structure, compact profile, and no need for additional filtering components. Meanwhile, it achieves a significantly wider impedance bandwidth compared with other antennas in the table. Although its realized gain is slightly lower than that of certain listed antennas, it is consistent with the average gain level of typical filtering antennas. This is primarily attributed to its low-profile single-layer structure, compact profile, the high-loss nature of the FR4 substrate, and the inherent properties of wideband patch antennas. Although some antennas in the literature attain a higher gain via multilayer structures, the proposed antenna achieves a more optimal balance between key performance metrics: low profile, compact size, impedance bandwidth, gain, and frequency selectivity.

5. CONCLUSION

This paper proposes a compact, wideband filtering patch antenna characterized by a simple structure and no requirement for additional filtering components. This antenna features a wide impedance bandwidth, a flat gain response within the passband, and high frequency selectivity. By adjusting the dimensions of the star-shaped slot on the upper layer and related parameters on the lower layer, the desired filtering performance was ultimately achieved. To validate the design principle, electromagnetic simulations are performed using High Frequency Structure Simulator (HFSS). Key performance parameters of the antenna including reflection coefficient, realized gain, and radiation pattern are analyzed, and a physical prototype of the antenna is fabricated for experimental testing and validation. Experimental results indicate that the antenna exhibits a -10 dB impedance bandwidth of 2.33–4.65 GHz and a peak realized gain of 4.25 dBi, along with excellent radiation characteristics across the entire passband. Owing to these advantages, the proposed filtering antenna holds broad application potential in 5G communication systems.

ACKNOWLEDGEMENT

This work was supported by the Fund of Anhui Mining Machinery and Electrical Equipment Coordination Innovation Center (Anhui University of Science and Technology) under grant No. KSJD202406.

REFERENCES

[1] Zuo, J., X. Chen, G. Han, L. Li, and W. Zhang, "An integrated approach to RF antenna-filter co-design," *IEEE Antennas and Wireless Propagation Letters*, Vol. 8, 141–144, 2009.

[2] Deng, J., S. Hou, L. Zhao, and L. Guo, "A reconfigurable filtering antenna with integrated bandpass filters for UWB/WLAN applications," *IEEE Transactions on Antennas and Propagation*, Vol. 66, No. 1, 401–404, 2018.

[3] Lu, Y., Y. Wang, S. Gao, C. Hua, and T. Liu, "Circularly polarised integrated filtering antenna with polarisation reconfigurability," *IET Microwaves, Antennas & Propagation*, Vol. 11, No. 15, 2247–2252, 2017.

[4] Hu, H.-T., F.-C. Chen, and Q.-X. Chu, "Novel broadband filtering slotline antennas excited by multimode resonators," *IEEE Antennas and Wireless Propagation Letters*, Vol. 16, 489–492, 2017.

[5] Wu, W.-J., Y.-Z. Yin, S.-L. Zuo, Z.-Y. Zhang, and J.-J. Xie, "A new compact filter-antenna for modern wireless communication systems," *IEEE Antennas and Wireless Propagation Letters*, Vol. 10, 1131–1134, 2011.

[6] Mao, C.-X., S. Gao, Y. Wang, Z. Wang, F. Qin, B. Sanz-Izquierdo, and Q.-X. Chu, "An integrated filtering antenna array with high selectivity and harmonics suppression," *IEEE Transactions on Microwave Theory and Techniques*, Vol. 64, No. 6, 1798–1805, 2016.

[7] Jin, J. Y., S. Liao, and Q. Xue, "Design of filtering-radiating patch antennas with tunable radiation nulls for high selectivity," *IEEE Transactions on Antennas and Propagation*, Vol. 66, No. 4, 2125–2130, 2018.

[8] Chuang, C.-T. and S.-J. Chung, "Synthesis and design of a new printed filtering antenna," *IEEE Transactions on Antennas and Propagation*, Vol. 59, No. 3, 1036–1042, 2011.

[9] Chu, H. and Y.-X. Guo, "A filtering dual-polarized antenna subarray targeting for base stations in millimeter-wave 5G wireless communications," *IEEE Transactions on Components, Packaging and Manufacturing Technology*, Vol. 7, No. 6, 964–973, 2017.

[10] Yang, W., J. Huang, D. Chen, K.-L. Yu, Q. Xue, and W. Che, "Broadband dual-polarized filtering metasurface-based antennas using characteristic mode analysis for 5G millimeter-wave applications," *IEEE Transactions on Antennas and Propagation*, Vol. 72, No. 5, 3912–3927, 2024.

[11] Cheng, G., B. Huang, Z. Huang, and L. Yang, "A high-gain circularly polarized filtering stacked patch antenna," *IEEE Antennas and Wireless Propagation Letters*, Vol. 22, No. 5, 995–999, 2023.

[12] Tang, M.-C., D. Li, Y. Wang, K.-Z. Hu, and R. W. Ziolkowski, "Compact, low-profile, linearly and circularly polarized filtennas enabled with custom-designed feed-probe structures," *IEEE Transactions on Antennas and Propagation*, Vol. 68, No. 7, 5247–5256, 2020.

[13] Li, L., H. D. Xiong, W. Y. Wu, A. B. Fu, and J. Y. Han, "A T-shaped strips loaded wideband filtering patch antenna with high selectivity," *IEEE Antennas and Wireless Propagation Letters*, Vol. 23, No. 1, 89–93, 2024.

[14] Chen, B.-J., X.-S. Yang, and B.-Z. Wang, "A compact high-selectivity wideband filtering antenna with multipath coupling structure," *IEEE Antennas and Wireless Propagation Letters*, Vol. 21, No. 8, 1654–1658, 2022.

[15] Dhwaj, K., J. M. Kovitz, H. Tian, L. J. Jiang, and T. Itoh, "Half-mode cavity-based planar filtering antenna with controllable transmission zeroes," *IEEE Antennas and Wireless Propagation Letters*, Vol. 17, No. 5, 833–836, 2018.

[16] Xu, K., J. Shi, X. Qing, and Z. N. Chen, "A substrate integrated cavity backed filtering slot antenna stacked with a patch for frequency selectivity enhancement," *IEEE Antennas and Wireless Propagation Letters*, Vol. 17, No. 10, 1910–1914, 2018.

[17] Hu, P. F., Y. M. Pan, X. Y. Zhang, and B.-J. Hu, "A filtering patch antenna with reconfigurable frequency and bandwidth using F-shaped probe," *IEEE Transactions on Antennas and Propagation*, Vol. 67, No. 1, 121–130, 2019.

[18] Yang, W., Y. Zhang, W. Che, M. Xun, Q. Xue, G. Shen, and W. Feng, "A simple, compact filtering patch antenna based on mode analysis with wide out-of-band suppression," *IEEE Transactions on Antennas and Propagation*, Vol. 67, No. 10, 6244–6253, 2019.

[19] Liu, Q. and L. Zhu, "A compact wideband filtering antenna on slots-loaded square patch radiator under triple resonant modes," *IEEE Transactions on Antennas and Propagation*, Vol. 70, No. 10, 9882–9887, 2022.

[20] Chen, X., Q. Zhuge, G. Han, R. Ma, J. Su, and W. Zhang, "A wideband harmonic suppression filtering antenna with multiple radiation nulls," *Progress In Electromagnetics Research Letters*, Vol. 112, 17–25, 2023.

[21] Mao, J., S. Zhou, J. Zhang, Y. Du, and J. Li, "A circularly polarized filtering patch antenna based on parasitic patches with slots," *Microwave and Optical Technology Letters*, Vol. 66, No. 11, e70042, 2024.

[22] Sun, Y. Q., Z. J. Zhai, D. H. Zhao, F. Lin, X. Y. Zhang, and H. J. Sun, "High-gain low cross-polarized dual-polarized filtering patch antenna without extra circuits," *IEEE Antennas and Wireless Propagation Letters*, Vol. 21, No. 7, 1368–1372, 2022.

[23] Cheng, G., J. Zhou, B. Huang, L. Yang, and Z. Huang, "Compact low-profile wideband filtering antenna without additional filtering structure," *IEEE Antennas and Wireless Propagation Letters*, Vol. 22, No. 10, 2477–2481, 2023.

[24] Yang, D., H. Zhai, and C. Guo, "A simple filtering patch antenna based on stub-loaded resonator," *Microwave and Optical Technology Letters*, Vol. 63, No. 7, 1920–1926, 2021.

[25] Yang, G., M. Li, L. Xiang, R. Xiao, Y. Qian, S. Qi, and W. Wu, "A slotline-fed wideband dipole with filtering gain response," *IET Microwaves, Antennas & Propagation*, Vol. 16, No. 13, 841–845, 2022.

[26] Hu, K.-Z., B.-C. Guo, S.-Y. Pan, D. Yan, M.-C. Tang, and P. Wang, "Low-profile single-layer half-mode SIW filtering antenna with shorted parasitic patch and defected ground structure," *IEEE Transactions on Circuits and Systems II: Express Briefs*, Vol. 70, No. 1, 91–95, 2023.